Dynamics and Scaling of Single DNA Molecules in Forces and Flows

William E. Uspal[1]
[1] *Massachusetts Institute of Technology, Cambridge, Massachusetts 02139, USA*
(Dated: May 16, 2008)

We numerically examine the extension of tethered worm-like chains in shear flow, obtaining agreement with scaling arguments that invoke thermal fluctuations and the specific nonlinearity of the WLC force law. The transient tension distribution is obtained and likewise found to reflect nonlinearity and finite extensibility. Cyclic dynamics of the chain free end are observed. Numerical simulations are also performed for electric field-driven WLCs colliding with mobile obstacles. Unhooking time is shown to agree with a theoretical model derived for stationary obstacles.

PACS numbers:

The past decade has seen intense research into the mechanics of single DNA molecules, motivated by potential biotechnological applications and the importance of DNA mechanics to cellular processes, e.g. viral packaging. [1] Optical trapping experiments have probed the phenomenological mechanical parameters, internal modes, and tension-induced phase transitions of DNA molecules. [2] DNA tethered to a substrate and stretched by an imposed shear flow is a potential testbed for single molecule flourescence microscopy experiments, such as could examine protein/DNA interaction kinetics and test the prevailing model for optimal genetic search. Doubly tethered chains could serve as electrical contacts for organic electronics. [3] Researchers have made scaling arguments for the extension of singly tethered chains in shear and probed chain statics and dynamics experimentally and computationally, revealing cyclic motion of the chain free end. [4] However, mapping a fluorescing protein to a local base pair requires clearer understanding of the chain conformation and tension profile. In this letter, we report some detailed results of Brownian Dynamics (BD) simulations of tethered worm-like chains in imposed shear flow.

Likewise, much recent attention has focused on the dynamics of single DNA molecules in confined geometries, such as are encountered in microfluidic devices. There is wide interest in a microfluidic "lab on a chip" replacement for conventional capillary gel electrophoresis systems for genome sequencing, which remains prohibitively costly for many envisioned medical therapies. [5] Researchers have examined the electrophoretic motion of confined DNA through lithographically patterned post arrays and dilute, quasi-two dimensional self-assembled arrays of superparamagnetic colloids. [6–8] In this connection, several groups have studied the dynamics of individual DNA/obstacle collisions, cataloguing and modeling various collision types. [7, 9] However, none have studied the collision of electrophoresing DNA with mobile, diffusing obstacles, whether free or confined to a potential well. In this letter, we discuss an analytical model for J-collision unhooking time and outline some BD investigations of DNA/mobile colloid collision dynamics.

Tethered Polymer in Shear: Scaling Laws

Brochard-Wyart modeled a chain tethered to a substrate in simple shear as a string of n blobs of size y. [10] The force of friction on each blob is $\gamma\eta y^2$, where γ is the shear rate and η is the solvent viscosity, giving a total force of

$$f(x) = \sum^{n} \eta\gamma y_i^2 = \int_0^x \eta\gamma(dx/y). \tag{1}$$

The Pincus rule determines blob length scale from the balance of applied force and thermal energy, giving

$$f(x) = \int_0^x \eta\gamma y(x')dx' = k_B T/y \tag{2}$$

and therefore, via the Leibniz rule, a blob height profile $y(x) = \sqrt{\frac{kT}{\eta\gamma}}$. Furthermore, blob theory gives the deformation dx/dn of a free chain under traction as

$$\frac{dx}{dn} = a\left(\frac{fa}{kT}\right)^{2/3}, \tag{3}$$

where a is the persistence length. Substituting $f(x) = kT/y(x)$ and integrating over the length L, we obtain

$$L = N^{3/2}a^{5/2}\left(\frac{\eta\gamma}{kT}\right)^{1/2} = R_F(\gamma\tau_z)^{1/2}. \tag{4}$$

However, this scaling argument ignores the role of thermal fluctuations. Attending to fluctuation of the chain free end, as Ladoux and Doyle did, leads to a different scaling exponent. [11] Moreover, their results depend on the specific form of the spring force law. They begin by citing a result from Hatfield and Quake [12] that gives the transverse spring constant of an extended chain: $k_\perp = f(R)/R$. This result is easily obtained by considering the force $f(\delta y)$ required for a displacement δy and expanding to first order in δy. Equipartition theorem gives $\frac{1}{2}k_\perp T^2 = k_B T$ and so

$$\delta y = (2k_B TR/F)^{1/2} \tag{5}$$

With the force on the chain given by the Marko-Siggia [13] worm-like chain interpolation formula

$$Fa/k_BT = \left[\frac{1}{4}(1-R/L)^{-2} - \frac{1}{4} + R/L\right], \qquad (6)$$

we define $\epsilon \equiv 1-R/L$ and take the highly stretched $\epsilon \to 0$ limit: $F \sim \epsilon^{-2}$. Therefore, transverse fluctuations scale as $\delta y \sim \epsilon$. The spring force must balance the hydrodynamic force $F = \zeta\gamma\delta y$, where ζ is the drag coefficient, giving a scaling

$$\epsilon \sim \gamma^{-1/3}. \qquad (7)$$

However, following the same procedure but with a freely jointed chain spring force, $F \sim \epsilon^{-1}$, we obtain

$$\epsilon \sim \gamma^{-2/3}. \qquad (8)$$

Speculatively, we suggest an analogy between the inapplicability of mean field results in statistical field theory in the presence of thermal fluctuations (within critical dimensions) and this dramatic change of scaling exponent upon consideration of thermal fluctuations.

Unhooking of a Chain from an Obstacle

Randall and Doyle catalog collision types as J, U, X ("extending") and W on the basis of hooked chain configuration. [9] Rare W collisions, as seen in Figure 1, typically have the two chain ends on the same side of the obstacle upon impact, often in the shape of W. Likewise, J and U collisions are named after their shapes; completely extended hooked configurations are taken to be U if the difference between the two arm lengths is only a small fraction of the total extension, and J otherwise. In X collisions, the short arm reaches its maximum length while the long arm is still unraveling as a freely convected coil. Randall and Doyle develop a model for the unhooking dynamics of J collisions, based on the assumption that tension in the chain relaxes on a time scale longer than chain unhooking time. The tension distribution is therefore frozen, like a constant extension rope. Neglecting Brownian motion, they write the Langevin equation for a bead:

$$\frac{d\boldsymbol{x}_n}{dt} = \frac{1}{\zeta_n}\boldsymbol{T}(\boldsymbol{x}_n) + \mu\boldsymbol{E} \qquad (9)$$

where $\boldsymbol{T}(\boldsymbol{x}_n)$ is the force due to spring force gradient. Summing over this equation, all spring forces but that of the pivot spring j T'_j cancel. For the short arm

$$j\zeta_n\left(\frac{dx_1}{dt} - \mu E\right) = -T'_j. \qquad (10)$$

Likewise, for the long arm,

$$(N_b - j)\zeta_n\left(\frac{dx_2}{dt} - \mu E\right) = -T'_j. \qquad (11)$$

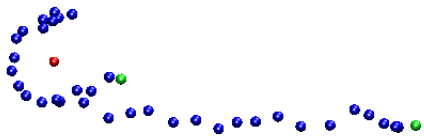

FIG. 1: A metastable W collision. Note that the chain ends, marked in green, are on the same side of the obstacle.

Here x_1 is the length of the short arm and x_2 is the length of the long arm. Because of the cancellation, the details of the chain tension distribution do not matter at this point. The foregoing equations may be subtracted and, using $dx_2/dt = -dx_1/dt$ and $j/N_b = x_1/L$, manipulated to obtain a simple differential equation:

$$\frac{dx_1}{dt} = -\mu E\left(1 - \frac{2x_1}{L}\right). \qquad (12)$$

This may be integrated as

$$t_{unhook}(x_1(0)) = \frac{-L}{2\mu E} ln\left(1 - \frac{2x_1(0)}{L}\right). \qquad (13)$$

Although they derive this unhooking time for a J collision, they find it holds for X collision data as well, because the retraction of the short arm governs the unhooking time. For a mobile obstacle, we modify Equation 9 to read

$$\frac{d\boldsymbol{x}_n}{dt} = \frac{1}{\zeta_n}\boldsymbol{T}(\boldsymbol{x}_n) + (\mu\boldsymbol{E} - \boldsymbol{v}_{obs}), \qquad (14)$$

and write $F_{obs} = 2T'_j$. After algebraic manipulation and integration, we obtain

$$t_{unhook}(x_1(0)) = \frac{-L}{2\mu E} ln\left(1 - \frac{2x_1(0)}{L}\right) - \frac{LN_b}{\zeta'\mu E}\left(\frac{x_1(0)^2}{L^2} - \frac{1}{2} ln\left(1 - \frac{2x_1(0)}{L}\right) + \frac{x_1(0)}{L}\right) \qquad (15)$$

Note that equations 13 and 15 are not yet nondimensional. Nondimensionalization gives a prefactor of $NL/2PeN_{k,s}$.

Numerical Method

We investigate both extension in shear and chain unhooking via Brownian Dynamics (BD). BD models chain time evolution via a set of n coupled Langevin equations:

$$d\boldsymbol{r}_j = \left[\boldsymbol{A} + \frac{1}{\zeta}(\boldsymbol{F}^s_j + \boldsymbol{F}^{ev}_j)\right]dt + \sqrt{\frac{2kT}{\zeta}}d\boldsymbol{W}_j \qquad (16)$$

for $j = 1, .., n$ beads connected by springs. ζ is the bead drag coefficient. The vector $\boldsymbol{A}$ is $\boldsymbol{v}$ for simulations in

shear and $\mu \boldsymbol{E}$ for simulations in an electric field; this is an example of hydrodynamic equivalence.

$\boldsymbol{F}_j^{ev}$ is an excluded volume force. For the tethered polymers we set $\boldsymbol{F}_j^{ev} = 0$, as $\epsilon \to 0$ and there is no significant overlap of adjacent beads. For chain/obstacle collisions, we use the soft, repulsive force proposed by Jendrejack et al.: [14]

$$F_j^{ev} = v k_B T N_{k,s}^2 \pi \left(\frac{3}{4\pi S_s^2}\right)^{5/2} \sum_{k=1,k\neq j}^{N} exp\left[-\frac{3}{4S_s^2}|\boldsymbol{r}_j - \boldsymbol{r}_k|^2\right](\boldsymbol{r}_j - \boldsymbol{r}_k) \quad (17)$$

Here $N_{k,s}$ is the number of Kuhn lengths per spring. For DNA, the Kuhn length b_k is twice the persistence length a, where $a = 0.053\mu m$. v is an excluded volume parameter. $S_s^2 = N_{k,s} b_k^2/6$ is the mean size of a Gaussian entropic spring of $N_{k,s}$ Kuhn segments.

$\boldsymbol{F}_j^s$ is the spring force, given by the Marko-Siggia force law:

$$\boldsymbol{F}_{spr} = \frac{k_B T}{2\lambda b_k}\left[(1 - Q/Q_0)^{-2} - 1 + 4Q/Q_0\right]\frac{\boldsymbol{Q}}{Q_0}, \quad (18)$$

Doyle and Underhill showed that to obtain the correct force-extension relationship, the Kuhn length b_k in the Marko-Siggia force law should be modified by a factor λ, which is determined by the number of persistence lengths per spring $N_{k,s}$. [15] This factor accounts for renormalization of the spring strength upon coarse-graining, and is chosen based on low, intermediate, or high applied force criteria, as no choice of λ can perfectly recapture the partition function. (It is likely that full-fledged renormalization analysis would reveal additional terms, e.g. a bending or three-body potential.) Underhill and Doyle provide numerical results for λ as a function of $N_{k,s}$ in these three regimes. These springs are finitely extensible with maximum extension Q_0; finite extensibility has been shown to have a significant impact on spring tension propagation in flow. [17]

Finally, $d\boldsymbol{W}_j$ is a noise term with $k = 1, .., n$ and correlations $\langle d\boldsymbol{W}_j(t)\rangle = 0$ and $\langle d\boldsymbol{W}_j(t) d\boldsymbol{W}_k(t')\rangle = dt\delta_{jk}\delta(t - t')\boldsymbol{\delta}$. For a free obstacle, we have another, strictly Brownian Langevin equation:

$$d\boldsymbol{r}_{obs} = \sqrt{\frac{2kT}{\zeta_{obs}}} d\boldsymbol{W}_{obs} \quad (19)$$

where $\boldsymbol{W}_{obs}$ is as above.

To step the bead-spring system forward in time, we use the semi-implicit predictor-corrector algorithm of Somasi et al., [16] while we use a simple Euler method to evolve the obstacle coordinates. To account for hard sphere repulsion of the substrate and of the obstacle, we employ the Heyes-Melrose displacement algorithm [18] after evolving the system as above. In the tethered polymer system, if we find a bead below $z = 0$, we displace it to $z = 0$. In the chain/obstacle system, we sample all beads in random order, and if a bead overlaps an obstacle of radius R_{obs}, we displace both along the vector connecting them such that their centers are separated by $R_{obs} + \delta$, where δ is a small distance. The displacements allocated to bead and obstacle are weighted by their respective values of $1/\zeta_{obs,bead}$. This algorithm is iterated until no moves are made, i.e. until bead displacement is self-consistent; the small value δ ensures that the algorithm converges after a reasonable number of iterations.

We nondimensionalize length by the maximum spring length Q_0 and time by $\zeta Q_0^2/(k_B T)$. For convenience, in the following we omit tildes and take variables to be nondimensionalized where appropriate. Prior to all simulations of chain dynamics, we generate Gaussian equilibrium coils by simulating the chains without a flow field or electric field for several Rouse relaxation times.

Tethered Polymer: Results and Discussion

We simulate λ-DNA at the dye concentration given in Ref 4, giving $L = 18\mu m$. As in Ref 4, we choose $n = 20$ beads, and therefore $N_{k,s} = 8.94$. We adopt a time step of 5×10^{-4}. We define dimensionless shear rate as the Weissenberg number $Wi \equiv \tau\gamma$, where τ is the longest relaxation time. We obtain τ for a chain of $n = 20$ beads by letting a chain relax from 30% extension and measuring the decay of $\langle \boldsymbol{RR}\rangle - \langle \boldsymbol{RR}\rangle_{eq}$, where $\boldsymbol{R}$ is the end-to-end vector. Figure 2 provides an example of such a relaxation measurement. For $Wi = 7.6$ and $\lambda = 1.25$, Figure 3 shows several tension profiles as a function of time, averaged over 1000 trajectories. For comparison, we show tension profiles at the same flow strength for a Hookean chain in Figure 4. Figure 5 depicts how the steady state fractional extension ϵ scales with Wi for $\lambda = 1$, $\lambda = 1.25$, and $\lambda = 1.6$, plotted with the data from the numerical simulations of Ref 11. The scaling exponents are calculated as -0.31 for our simulations and -0.37 for the simulations of Ref 11. In the steady state, we observe the cyclic dynamics of the chain free end described in Ref 4.

From comparison of Figures 3 and 4, we see that the nonlinearity and finite extensibility of the worm-like chain plays a significant role in chain statics and dynamics. Tension propagation is slowed and extension with shear weaker.

The exponent describing the scaling of ϵ with Wi is shown to be insensitive to choice of effective persistence length parameter λ. This is to be expected; small variation of coupling strength should not affect scaling exponents. Our exponent of -0.31 is closer to the predicted value of $-1/3$ than the value of -0.37 given by the simulations of Ref 11. This is likely due to the choice of excluded volume potential in Ref 11, which must be char-

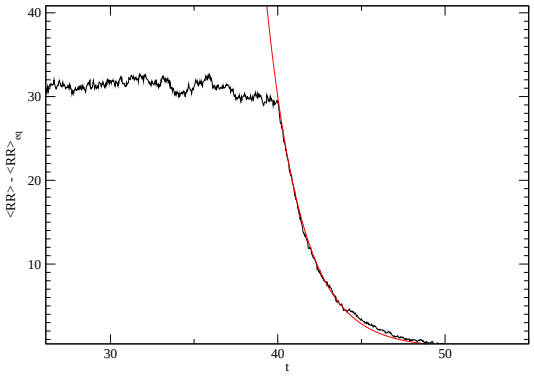

FIG. 2: Relaxation of $\lambda = 1.25$, $n = 20$ from 30% extension for an ensemble of 100 trajectories.

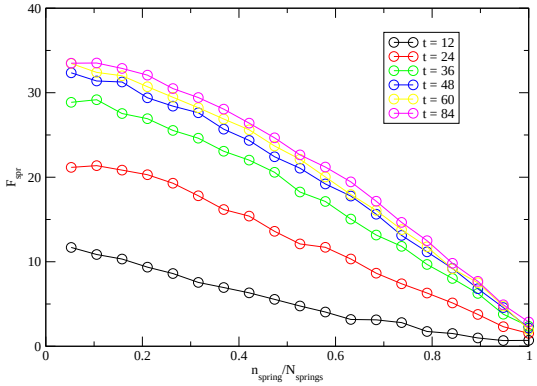

FIG. 3: Tension profile as a function of time for a WLC with $\lambda = 1.25$, $Wi = 7.6$ and $n = 20$ for an ensemble of 1000 trajectories.

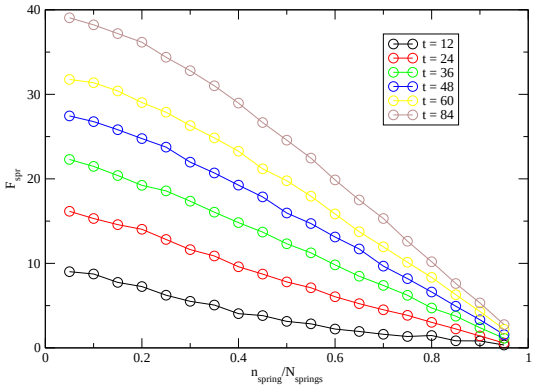

FIG. 4: Tension profile as a function of time for a Hookean chain with $n = 20$ and the same flow conditions as in Figure 3 for an ensemble of 1000 trajectories.

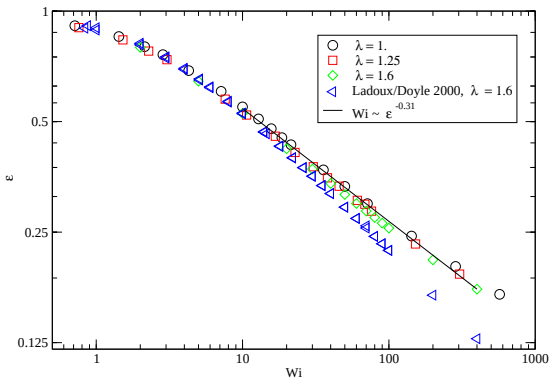

FIG. 5: Scaling of ϵ with Wi for ensembles of 100 trajectories for various values of λ, plotted with data from Ref 11.

acterized by a bead/substrate distance ξ, thereby leading to a larger shear force on the bead and greater stretching. This effect would be especially pronounced for high Wi, as chains are highly stretched and lie close to the substrate in this regime.

The cyclical dynamics of the chain free end are explained in Ref 4. A fluctuation in the y direction exposes the chain to a stronger flow, leading it to stretch. As it stretches, it drifts back toward the substrate, leading to retraction. In the course of cyclic dynamics, the distance between our chains and the substrate shrinks to nanometers, suggesting that the ionic structure of the substrate Debye layer may have an important effect, and could possibly be exploited to tune chain stretch. We intend to include such a potential in future simulations.

While scaling is insensitive to λ, for reasons discussed above the modified Marko-Siggia equation cannot possibly correctly capture the details of force-extension relationship over all force regimes. For that reason, we intend to implement an alternative, exact force law derived by Underhill and Doyle. [19]

Unhooking Dynamics: Results and Discussion

We simulate λ-DNA, for which $L = 20.5\mu m$, and adopt the discretization level $n = 38$, giving $N_{k,s} = 5.23$ Kuhn lengths per spring. From Underhill and Doyle, we have $\lambda = 1.91$, using the low force criterion. For the excluded volume parameter, we take $v = 0.0004\mu m^3$, as this value was shown by Kim and Doyle to correctly reproduce the λ-DNA radius of gyration. [20] We take our time step to be 1.25×10^{-4}; we must adopt this small time step, with stiff computational performance penalty, to avoid hav-

ing the predictor-corrector method return overstretched springs. We take the hard sphere volume of the obstacle to be $R_{obs} = 0.5$ and $\delta = 0.05$. Beads are assumed to have no hard sphere volume. We nondimensionalize the electric field strength by defining a Peclet number $Pe = \frac{\mu_0 E n \zeta a}{k_B T}$. For all simulations we take $Pe = 10$. The obstacle introduces a new drag coefficient ζ_{obs}, requiring definition of a new dimensionless group $\zeta' = \zeta_{obs}/\zeta$. We investigate $\zeta' = 5$, $\zeta' = 10$, and $\zeta' = \infty$.

Equilibrium coils are released a distance $l = 7$ upstream of the obstacle with impact parameter $b = 0$. The arbitrary choice of l only affects probability of collision, not the statistics of collision events. At each time step we check for a collision event, defined as the presence of chain beads in all four quadrants defined by a coordinate system attached to the obstacle. For trajectories with collisions, we record the unravel time, defined as the time from collision at which the short arm is at its maximum length. Unfortunately, there is no easy algorithm for automated recognition of this event; beads may fluctuate past the plane separating the long and short arms, for instance, making spatial location an inadequate criterion. W collisions make recognition based on chain connectivity difficult. We determine this time using visualization software, with which we also classify the type of collision. We also record the chain free time, defined as the first time from collision at which all chain beads are in the right half plane of the obstacle coordinate system. The unhooking time is defined as the difference between the free and unravel times.

For 25 trajectories with $\zeta' = \infty$, we observed eleven J/U collisions (44%), nine X collisions (36%), three W collisions (12%) and two non-collisions (8%). For 25 trajectories with $\zeta' = 10$, we observed six J/U collisions (24%), five X collisions (20%), two W collisions (4%), nine non-collisions (36%), and three "P" or "catch and release" collisions in which the obstacle was caught in a transient pocket before diffusing away. (Figure 6) In P collisions, the chain is typically oriented transverse to the field before obstacle release. Finally, for 17 trajectories with $\zeta' = 5$, we observed six J/U collisions (35%), one X collision (6%), one W collision (6%), eight non-collisions (47%) and one P collision (6%).

We show t_{unhook} plotted against short arm length $x_1(0)$ in Figure 7. Remarkably, data collapses onto the theoretical curve in Equation 13 for all values of ζ', even though Equation 13 was derived for a stationary obstacle. The correction in Equation 15 is manifestly not applicable to our simulation results. This, however, may be due to the inclusion of obstacle Brownian motion, which was not considered in the derivation of Equation 15. In writing $\boldsymbol{v}_{xobs} = 2T'_j/\zeta_{obs}$, we assumed that the only force on the obstacle is exerted by the pivot spring, but a noise term represents the force of solvent. Therefore, we plan on running simulations in which obstacle motion is limited to hard sphere displacement.

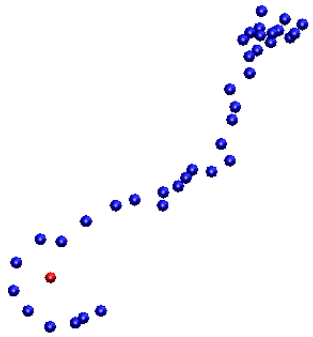

FIG. 6: A transient "pocket" configuration.

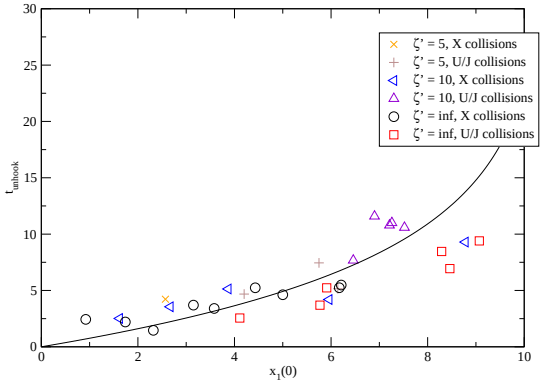

FIG. 7: Unhooking time as a function of short arm length after unraveling, with Equation 13 drawn as a solid line.

Even if obstacle mobility has no impact on unhooking dynamics, electrophoretic dispersivity may still be affected, as chain hold-up time is due to both unhooking and motion of the chain center of mass. Obviously the latter is significantly affected by ζ', as highly mobile obstacles may be dragged for considerable distances downfield. Hold-up time is defined with respect to the affine or free electrophoretic motion of the chain; it is the offset between linear fits to the approach and release trajectories. We intend to measure hold-up time for $\zeta' = 5$ and $\zeta' = 10$ and compare to $\zeta' = \infty$ data. We also plan on extending the hold-up model in Ref 9.

P collisions were not observed for stationary obstacles. The transient transverse orientation of the chain is interesting and warrants further investigation. Speculatively, if P collisions predominate for a particular ζ' regime, then chain motion through a field of such obstacles might have a steady state in which the loss of trapped obstacles to diffusion is counterbalanced by the gain of the obstacles in the area swept out by the chain, which would thereby retain its transverse orientation. The "wake" of the chain would be depleted of obstacles, which would diffuse down

the concentration gradient behind the chain. Motion of electrophoresing chains may be coupled by their effects on the obstacle field, even if they are hydrodynamically free draining. Even more speculatively, if obstacle drag scales with chain length in the right fashion, this could provide a new mechanism for DNA size separation.

Finally, we plan on running more simulations for an obstacle harmonic potential V; such a potential could represent a 2D lattice restoring force, the restoring force of a gel fiber under constant tension, etc.

Conclusions

In this letter, we outlined some preliminary results from Brownian Dynamics simulations of tethered wormlike chains stretching in shear flow and electrophoresing WLCs colliding with mobile obstacles. We obtained the tension distribution and scaling of ϵ with Wi for the tethered chains, and for the colliding chains we found that Equation 13 describes stationary and mobile, diffusing obstacles equally well. These results warrant continued study, and we outlined future investigations: consideration of the effect of ionic electrostatic forces on the tethered chain, investigation of electrophoresis hold-up time, study of the P collisions, and consideration of an obstacle harmonic restoring force. These investigations may allow finer control of chain orientation and stretch, and therefore lead to improved microfluidic devices for such applications as gene mapping and genome sequencing.

[1] C. Bustamante, Z. Bryant, and S.B. Smith, Nature **421**, 423 (2003).

[2] S.B. Smith, Y. Cui, and C. Bustamante, Science **271**, 795 (1996).

[3] C.A. Lueth and E.S.G. Shaqfeh, Korea-Australia Rheology J. **19**, 141 (2007).

[4] P.S. Doyle, B. Ladoux, and J.-L. Viovy, Phys. Rev. Lett. **84**, 4769 (2000).

[5] J.-L. Viovy, Rev. Mod. Phys. **72**, 813 (2000).

[6] A. Mohan and P.S. Doyle, Macromolecules **40**, 8794 (2007).

[7] E.M. Sevick and D.R.M. Williams, Phys. Rev. Lett. **76**, 2595 (1996).

[8] O.A. Hickey and G.W. Slater, Phys. Lett. A **364**, 448 (2007).

[9] G.C. Randall and P.S. Doyle, Macromolecules **39**, 7734 (2006).

[10] F. Brochard-Wyart, Europhys. Lett. **23**, 105 (1993).

[11] B. Ladoux and P.S. Doyle, Europhys. Lett., **52**, 511 (2000).

[12] J.W. Hatfield and S.R. Quake, Phys. Rev. Lett. **82**, 3548 (1999).

[13] J.F. Marko and E.D. Siggia, Macromolecules **28**, 8759 (1995).

[14] R.M. Jendrejack, J.J. de Pablo and M.D. Graham. J. Chem. Phys. **116**, 7752 (2002).

[15] P.T. Underhill and P.S. Doyle, J. Non-Newtonian Fluid Mech. **122**, 3 (2004).

[16] M. Somasai *et al.*, J. Non-Newtonian Fluid Mech. **108**, 227 (2002).

[17] A. Mohan and P.S. Doyle. Macromolecules **40**, 4301 (2007).

[18] D.M. Heyes and J.R. Melrose. J. Non-Newtonian Fluid Mech. **46**, 1 (1993).

[19] P.T. Underhill and P.S. Doyle, J. Rheol. **50**, 513 (2006).

[20] J.M. Kim and P.S. Doyle, Macromolecules **40**, 9151 (2007).